Upper mantle velocity structure beneath Italy from direct and secondary *P*-wave teleseismic tomography

Giovanni Battista Cimini and Pasquale De Gori
Istituto Nazionale di Geofisica, Roma, Italy

Abstract
High-quality teleseismic data digitally recorded by the National Seismic Network during 1988-1995 have been analysed to tomographically reconstruct the aspherical velocity structure of the upper mantle beneath the Italian region. To improve the quality and the reliability of the tomographic images, both direct (P, PKP_{df}) and secondary (pP, sP, PcP, PP, PKP_{bc}, PKP_{ab}) travel-time data were used in the inversion. Over 7000 relative residuals were computed with respect to the IASP91 Earth velocity model and inverted using a modified version of the ACH technique. Incorporation of data of secondary phases resulted in a significant improvement of the sampling of the target volume and of the spatial resolution of the heterogeneous zones. The tomographic images show that most of the lateral variations in the velocity field are confined in the first ~250 km of depth. Strong low velocity anomalies are found beneath the Po plain, Tuscany and Eastern Sicily in the depth range between 35 and 85 km. High velocity anomalies dominate the upper mantle beneath the Central-Western Alps, Northern-Central Apennines and Southern Tyrrhenian sea at lithospheric depths between 85 and 150 km. At greater depth, positive anomalies are still observed below the northernmost part of the Apenninic chain and Southern Tyrrhenian sea. Deeper anomalies present in the 3D velocity model computed by inverting only the first arrivals dataset, generally appear less pronounced in the new tomographic reconstructions. We interpret this as the result of the ray sampling improvement on the reduction of the vertical smearing effects.

Key words *direct and secondary P phases – travel-time residuals – upper mantle tomography*

1. Introduction

Recent tomographic reconstructions of the seismic velocity field in the upper mantle beneath Italy have attested the strong lateral heterogeneity of the lithosphere-asthenosphere system in this tectonically very complex area (Babuška and Plomerová, 1990; Spakman, 1990; Amato *et al.*, 1993a; Cimini and Amato,

1993; Spakman *et al.*, 1993). From these investigations, characterized by different inversion techniques, model parameterization and dataset of seismic phase used, a common, although somewhat controversial, result has emerged: the existence of a nearly continuous subduction system below the whole Italian region. This evidence emerges from the intepretation, in terms of mantle structural features, of the strong and broad positive velocity anomalies imaged at different depths beneath Italy from the Alps to the Tyrrhenian sea. In Northern Apennines and Southern Tyrrhenian sea, the presence of a subducting lithosphere is corroborated by the occurrence of subcrustal seismicity with spatial distribution corresponding quite well with the velocity perturbation patterns (Amato *et al.*, 1993b; Giardini and Velonà,

1991; Selvaggi and Amato, 1992). The wide region of high velocity anomalies detected beneath the Alps has been interpreted with the presence of deep apparently aseismic lithospheric roots linked to the continental collision between the Eurasian and Adriatic plates (Panza and Mueller, 1979; Babuška and Plomerová, 1990; Spakman, 1990; Cimini and Amato, 1993).

However, despite the efforts undertaken to provide more and more reliable images of the deep structure of Italy and, more in general, of the Mediterranean region, large uncertainties still exist on the geometry, extension and continuity at depth of the subducted lithosphere. Even considering the different scale of spatial resolution, the misfit in the seismic structure recovered by the above mentioned tomographic studies (see the 3D velocity model in Amato *et al.*, 1993a and model EUR89B in Spakman *et al.*, 1993 for a comparison) suggests to proceed very cautiously in the geodynamic interpretation of the tomographic reconstructions. This misfit, we believe, is mainly due to the approximate experimental condition in which the tomographic problem is usually performed, namely inhomogeneous station coverage, poor seismic data quality and inadequate sampling of the target volume. Particularly the heterogeneous sampling of the Earth structure by the seismic ray paths may have severe consequences on the reliability of tomographic reconstructions, resulting in low resolution images of large regions of the deep structure under investigation. Lack of resolution can, for instance, lead to spurious mapping of the existing velocity perturbations with *smearing* in the predominant directions of illumination (Spakman *et al.*, 1989; van der Hilst and Spakman, 1989; Evans and Achauer, 1993).

In this study, starting from a dataset of well-recorded teleseismic waveforms, we explore the applicability of incorporating travel-time residual data of secondary *P* phases in a 3D inversion for the upper mantle velocity structure of Italy. The aim is to obtain a more complete sampling of the anomalies and a more accurate reconstruction of their shapes, especially in those areas not adequately sampled by direct *P*

rays from available source-receiver combinations. Inclusion of data of later arriving *P* phases can improve the spatial resolution of tomographic models because they sample Earth structure not sampled by direct *P* phases. Also, they enhance the density of intersections in the sampled volume adding rays that are oblique to rays of direct phases (van der Hilst and Engdhal, 1991).

2. Teleseismic data and method of analysis

The data that we used derive from 107 teleseisms digitally recorded by the National Network (RSNC) of the Istituto Nazionale di Geofisica (ING) in the last eight years. At present, the network is composed of more than 80 seismic stations equipped with mostly vertical short-period (1 Hz) seismometers (fig. 1). Signals from the seismic sites are transmitted via telephone lines to the central observatory in Rome, where they are A-D converted at a sampling rate of 50 *sps*. Two main requirements were adopted to select from the whole collection of teleseismic waveforms recorded by the RSNC stations during 1988-1995 the dataset used in this study. First, we examined the sources distribution of the available earthquakes in order to obtain a homogeneous dataset of both backazimuths and slownesses of teleseismic rays. Figure 2 shows the geographical distribution of the epicenters of the selected *P* ($30° \leq \Delta \leq 100°$) and *PKP* ($\Delta \geq 110°$) events. Second, we looked at the quality of the teleseismic waveforms to reduce the effect that large reading errors have on the ACH inversion procedure, which performs an L_2 norm minimization of the residual data (Aki *et al.*, 1977; Menke, 1989; Evans and Achauer, 1993). To do this we used an interactive graphic procedure that performs band-pass filtering, amplitude and time scaling, and alignment of the recordings of a teleseismic event. For each phase arrival the waveform alignment is performed by means visual correlation of the first two-three cycles of the relative wave train (fig. 3). Travel times of first arrivals (*P* and PKP_{df}) and of later arriving phases with very clear onsets (for instance *pP* and *sP* arrivals
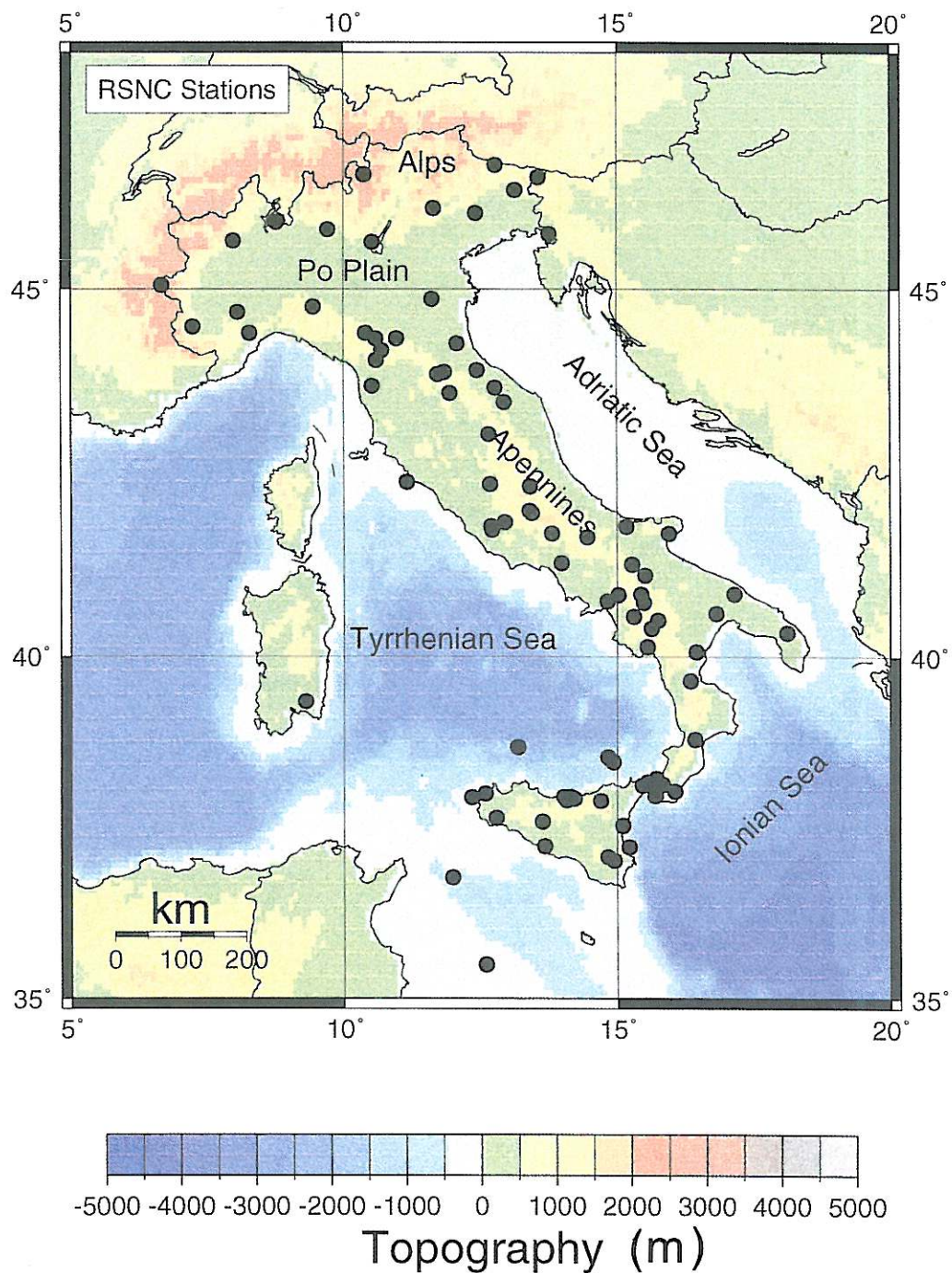
Fig. 1. Station distribution of the National Network (RSNC) of the Istituto Nazionale di Geofisica (ING).
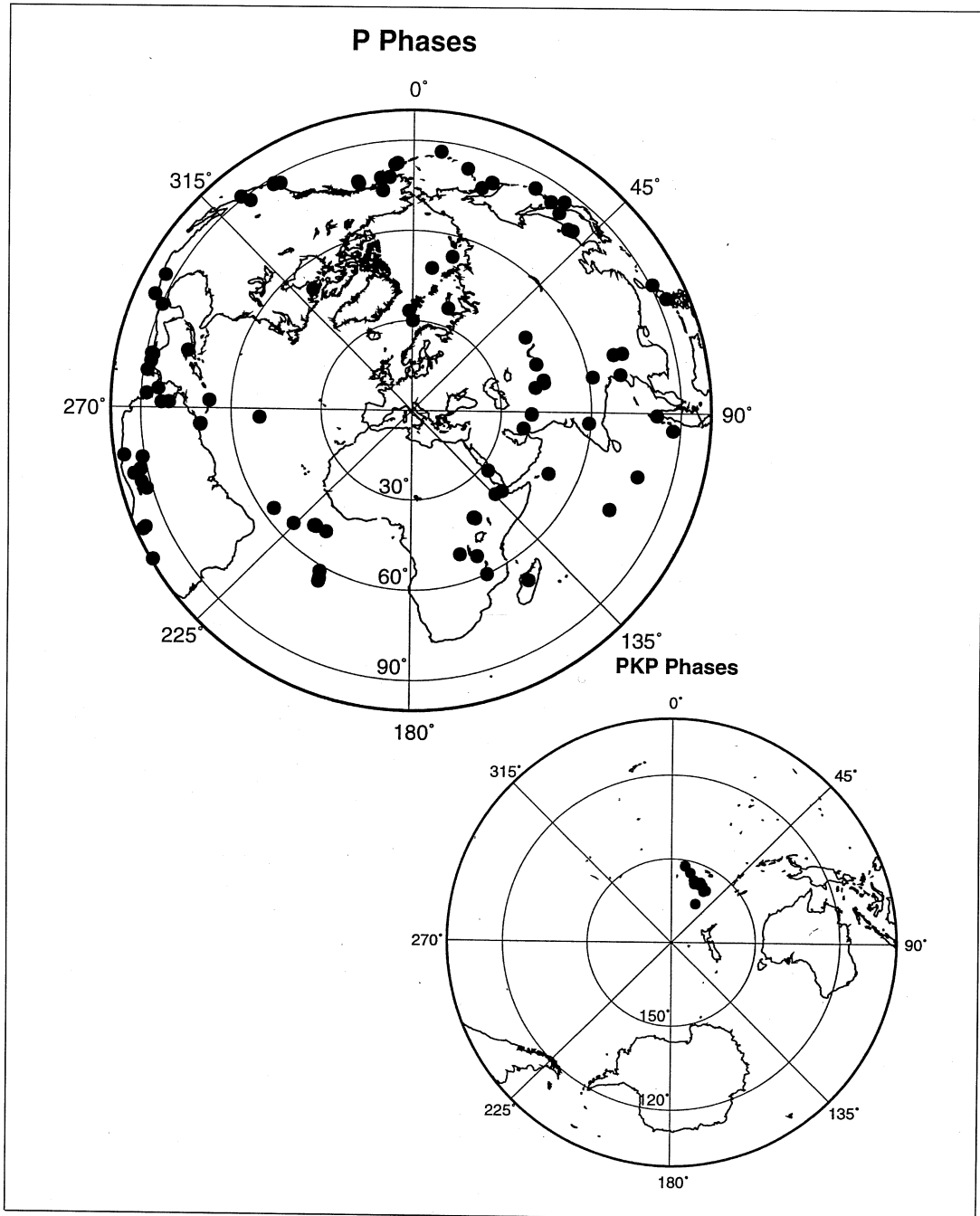
Fig. 2. Azimuthal equidistant maps of epicenters of the P ($30° \leq \Delta \leq 100°$) and PKP ($\Delta \leq 110°$) events used in this study.
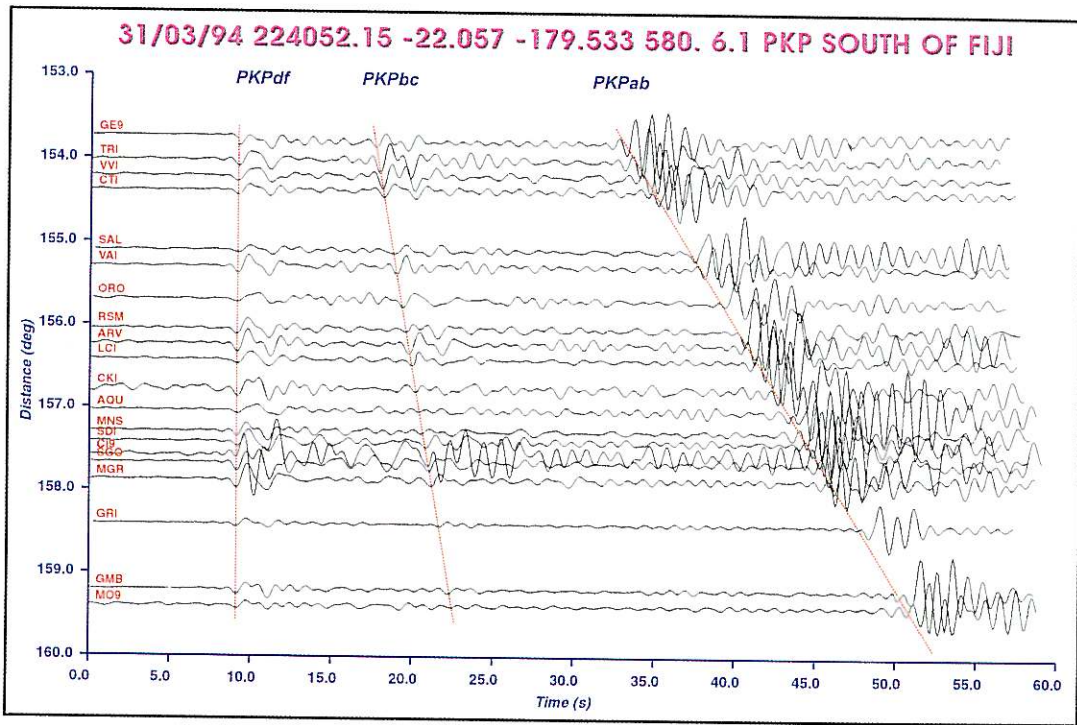
Fig. 3. Record section of the March 31, 1994, south of Fiji islands earthquake (m_b = 6.1) recorded at 20 stations of the Italian short-period seismic network. The seismograms are filtered in the frequency band 0.2 ÷ 2.0 Hz using a cosine taper on the low and high ends of the spectrum. The straight lines indicate the selected picking times of the various phases observed.

from deep earthquakes) were generally picked in correspondence of the first peak or trough of the wave train. For secondary arrivals characterized by more complex shapes we timed the digital seismograms in correspondence with the maximum amplitude of the wavelet. Weights based on the quality of the arrival time pick were assigned to the observed travel-time to account for the different reading uncertainty level or to discard (weight set to zero) low-quality data in the relative residual computation. The weighting factors used, 1.00, 0.75, 0.50, and 0.25, correspond to a picking accuracy of approximatively 0.10 s, 0.15 s, 0.20 s, and 0.25 s.

Following these selection criteria we collected 4420 seismograms that we accurately analysed to achieve a high precision in the computation of the arrival times of both direct and later arriving *P* phases. Figure 3 shows the seismogram alignment obtained by our picking procedure for a *PKP* event with epicenter in the Fiji islands region (range = 158°, azimuth = 31°). Figure 4 plots the observed travel times for three selected depth intervals after correction for the ellipticity of the Earth (Dziewonski and Gilbert, 1976), station elevation, and near-surface geology. The travel times of *pP* and *sP* phases, and of the surface-reflected *PP* phases were also corrected for the topography/bathymetry of reflection points (van der Hilst and Engdahl, 1991). In table I we list for each phase the number of observations used in the 3D inversion, the limits in the epicentral distance adopted in the selection process and the standard deviations σ_{rel} and σ_{pick} of the rela-

179

Mantle Phases - Crustal Sources

Mantle Phases - 100 km Sources

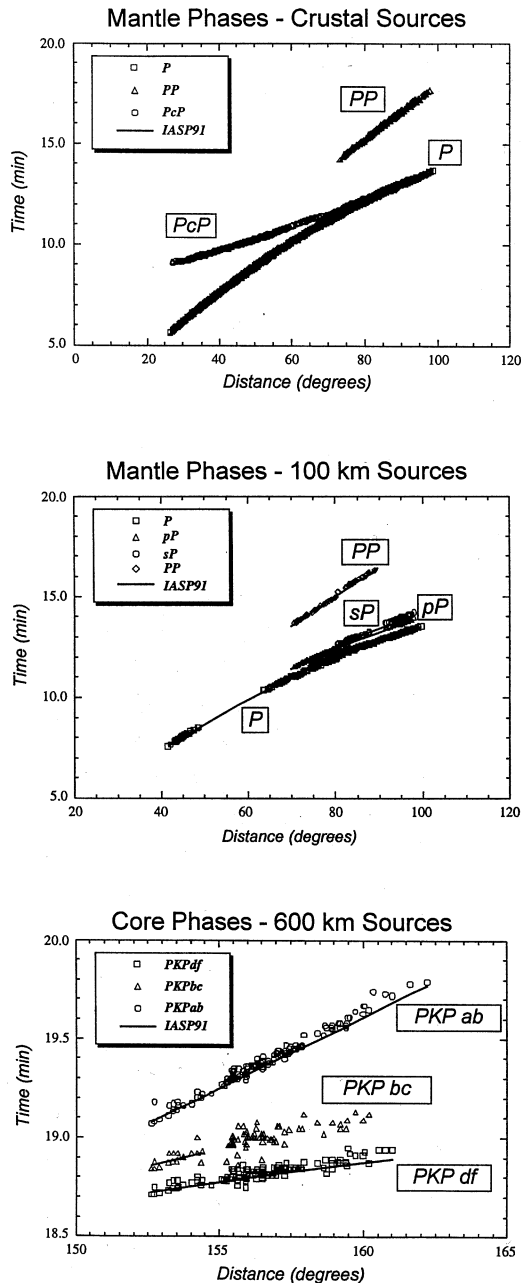## Core Phases - 600 km Sources

Fig. 4. Travel times picked from the observed *P* phases. Superimposed on the travel times are the interpretation of the phases and the curves showing predicted arrival times based on the IASP91 Earth velocity model (Kennett and Engdahl, 1991).

tive residuals. σ_{rrel} is the standard deviation computed for all the arrivals of a given phase, while σ_{pick} is a measure of the residual variation for events incoming from the same source region. The σ_{pick} values are determined under very similar experimental conditions (same set of seismic stations used, earthquake hypocenters localised in a small volume compared to the teleseismic distances), so they provide an estimate of the picking accuracy for the various phases. The largest σ_{pick} is observed for *PP* phases, thus confirming its intrinsic complexity. *PP* follows a mini-max travel-time path (for $\Delta < 180°$), and its waveform is phase-shifted by $\pi/2$ upon touching an internal caustic (Hill, 1974; Choy and Richards, 1975). This phase shift, although smaller for short-period data (van der Hilst and Engdahl, 1991), distorts an impulsive *P* pulse into an emergent (Hilbert transformed) *PP* onset. Also, the reflections at the surface other than the free surface (for example at some crustal interface or at Moho) contribute to complicate *PP* waveforms, making them more difficult to pick. Nevertheless, *PP* are very useful for increasing the range of incidence angles, adding rays that are more horizontal than direct *P* rays from near events.

We computed travel-time residuals by using the IASP91 velocity model (Kennett and Engdahl, 1991) as reference model. To do this, we utilized the $\tau(p)$ (p is the ray parameter) computation scheme described in Buland and Chapman (1983). Relative residuals were determined in order to minimize errors in hypocentral mislocations, origin time determinations, and path effects outside the modelling space. They were formed by subtracting the weighted mean residual for the given event and phase from the absolute residuals computed for each observation (Cimini *et al.*, 1994). Figure 5 shows the polar diagrams of the relative residuals observed at three stations of the RSNC located in the Western Alps (DOI), Northern Apennines (PGD), and Calabrian arc (ATN), respectively. These examples are representative of the strong directional dependence of the travel-time residuals of both first and secondary *P* phases. The observed residual patterns are consistent with large velocity gradi-

Table I. Residual statistics and selection criteria for the seismic phases analysed.

Phase	N. obs.	σ_{rrel} (s)	Δ_{min} (°)	Δ_{max} (°)	σ_{pick} (s)
P	3842	0.72	25	98	0.05
pP	655	0.75	25	98	0.14
sP	1110	0.73	25	98	0.14
PcP	397	0.86	25	98	0.12
PP	364	0.87	50	180	0.20
PKP_{df}	393	0.64	110	180	0.12
PKP_{bc}	58	0.59	145	155	0.18
PKP_{ab}	251	0.73	145	175	0.15

ents in the lithosphere-asthenosphere system beneath the three stations. In the next section, summarizing the results of the application of the ACH inversion on these data (see Cimini and Amato, 1993; Evans and Achauer, 1993 for details on the proper use of this technique), we show images of the upper mantle velocity structure below Italy. These tomographic reconstructions allowed us to delineate the extent, geometry, and spatial resolution of the main heterogeneous zones.

3. Inversion results

Figures 6a-c display the three-dimensional *P*-velocity structure of the lithosphere-asthenosphere system of Italy obtained by inverting the $P+PKP_{df}$ dataset (4235 travel-time residuals; panels on the left) and the *All Phases* dataset (7070 travel-time residuals; panels on the right). The *All Phases* dataset includes the $P+PKP_{df}$ dataset and 2835 travel-time residuals of later arriving phases. The lateral heterogeneities are modeled as velocity perturbations relative to a starting model built up of a crustal layer (0-35 km) overlying six homogeneous layers with horizontal block dimensions ranging from 50×50 km (layer 2) to 100×100 km (layer 7). The crustal layer (layer 1, not represented in fig. 6) consists of station cones with aperture defined by the rays that from the base of the crust, located at 35 km of depth, reach

the stations. The mapped velocity changes represent the average of four different inversions performed with the use of an offset – and – averaging algorithm to avoid artifacts due to the block boundaries (Evans and Achauer, 1993). Some representative parameters of the inversion of the two datasets are listed in table II. For both the $P+PKP_{df}$ and the *All Phases* inversion we used the same damping parameter (50 s^2) to allow a straightforward comparison of the tomographic results. The choice was made by computing the trade-off curve between the residual variance and the model length for the $P+PKP_{df}$ dataset. As a consequence, part of the greater unmodelled data variance (remaining variance) observed after inversion of the *All Phases* dataset may be due to the non-optimal value for this dataset of the selected damping parameter.

In layer 2 (35-85 km; fig. 6a, upper panels), strong lateral variations in the velocity field with respect to the initial value of 8.05 km/s are imaged below the Central-Western Alps, Northern Apennines, and Southern Tyrrhenian sea-Calabrian arc, as positive anomalies ($+5 \div +7\%$), and beneath the Po plain, Tuscany, and Central-Northeastern Sicily as negative anomalies ($-4 \div -7\%$). These velocity anomalies are recovered by both inversions; their spatial distribution is consistent with results of previous tomographic studies (Cimini and Amato, 1993). In particular, the positive anomaly beneath the crust of the westernmost
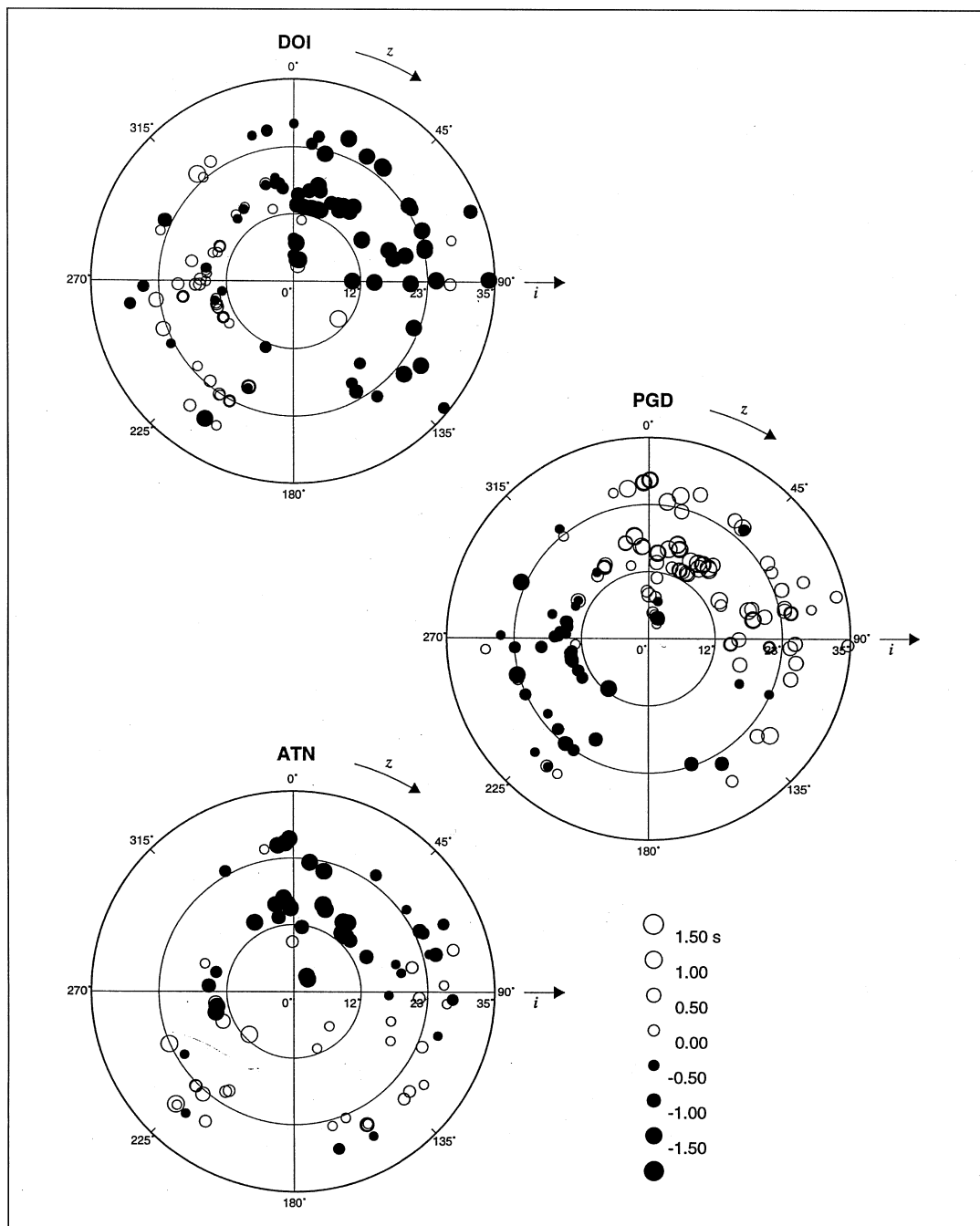
Fig. 5. Spatial distribution of relative residuals (s) for three seismic stations of the Italian network, *versus* azimuth and incidence angle of the approaching teleseismic rays.
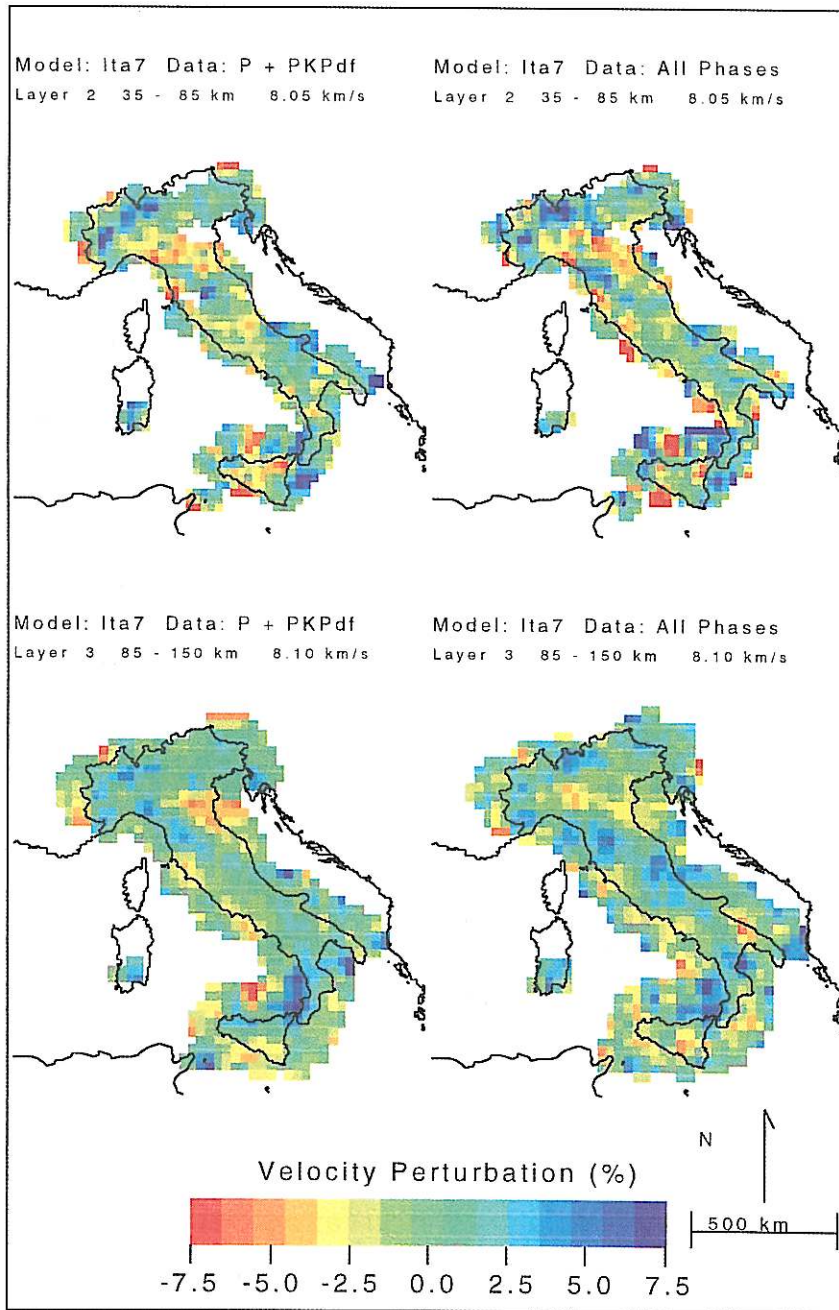
Fig. 6a. A comparison between the two *P*-wave velocity models for the upper mantle structure of Italy obtained by 3D inversion of the $P+PKP_{df}$ (left panels) and *All Phases* datasets (right panels): 35-85 km, 85-150 km.

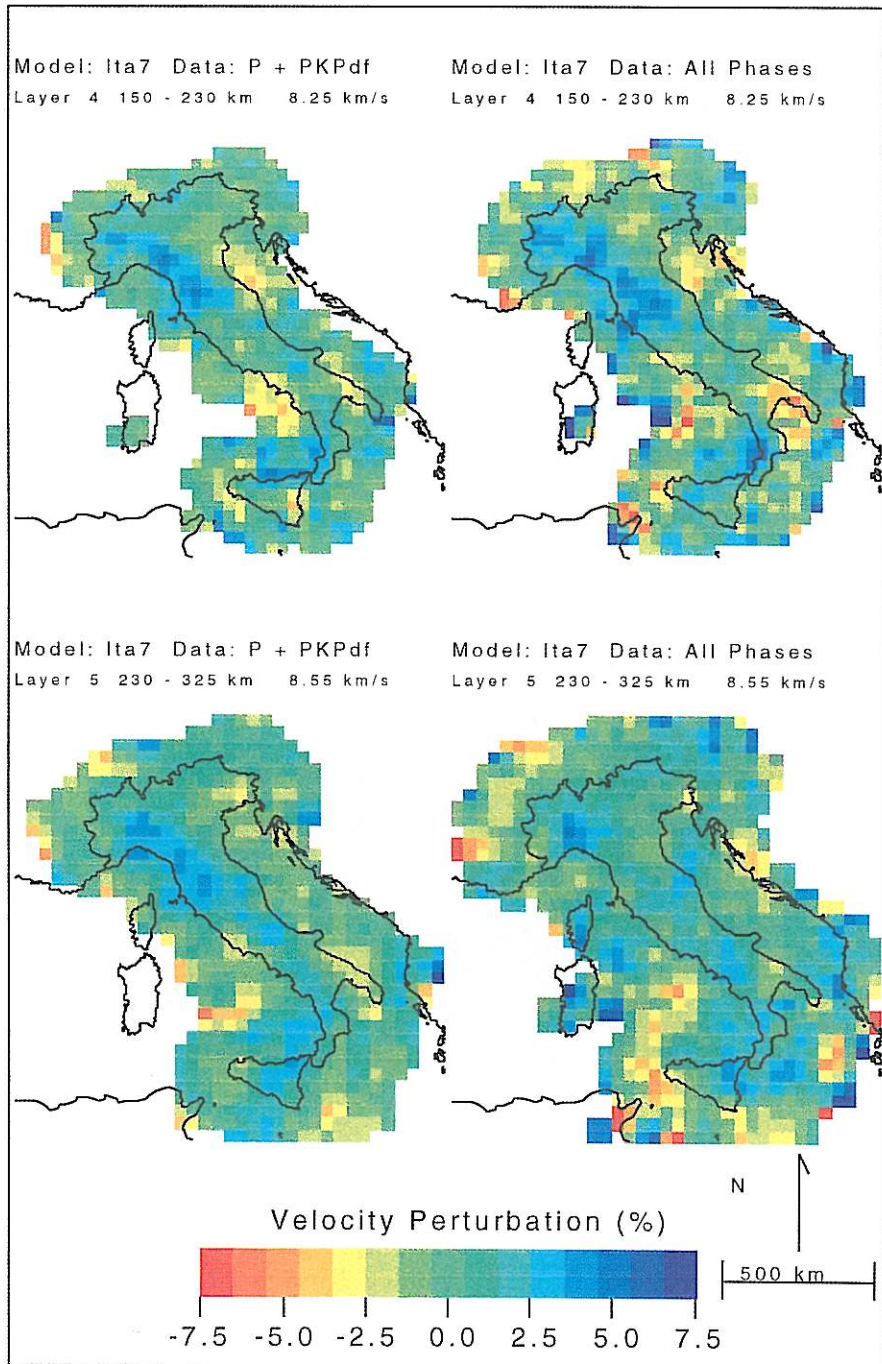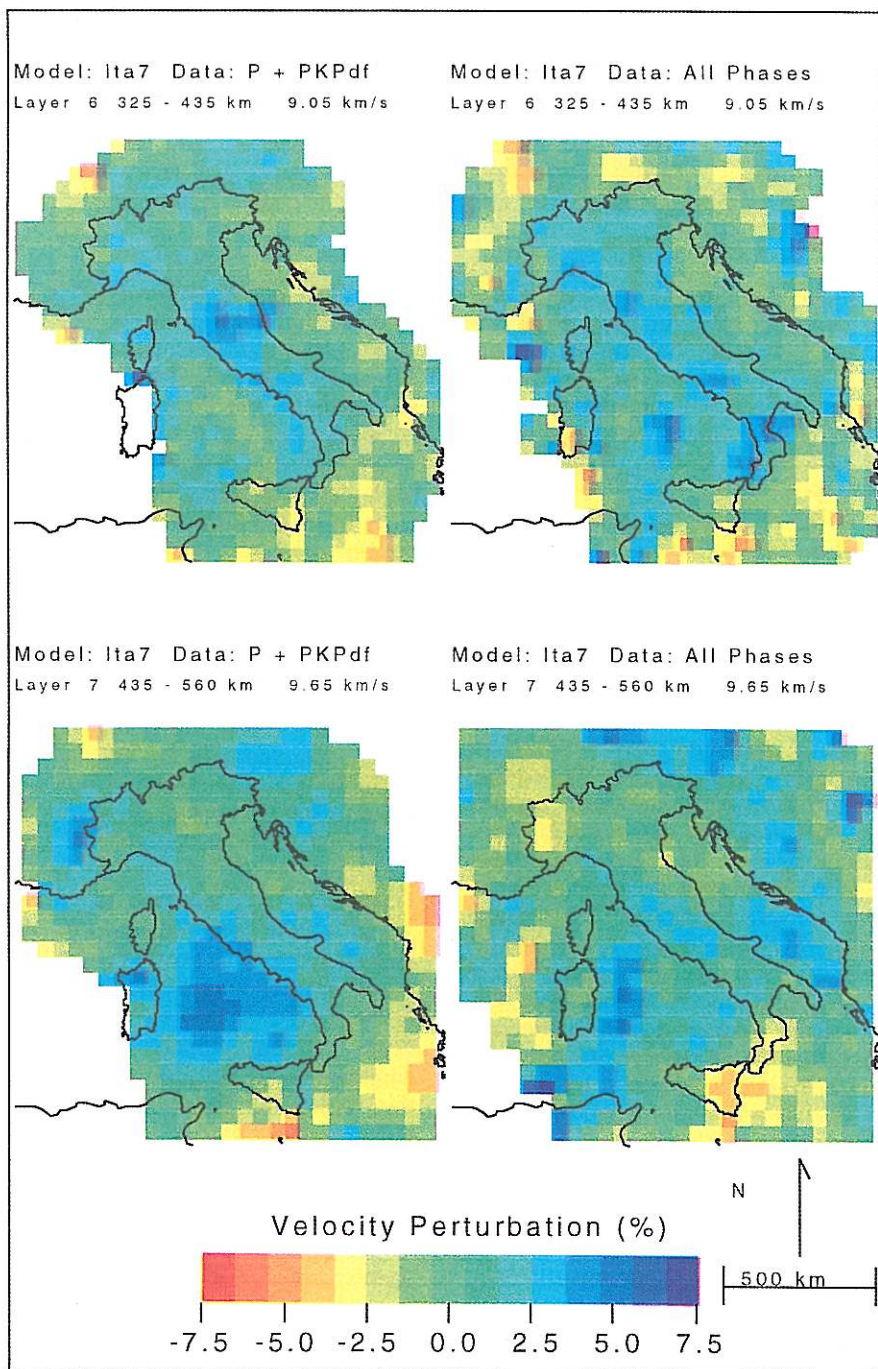**Fig. 6b.** Same as fig. 6a for the depth intervals 150-230 km and 230-325 km.

Fig. 6c. Same as fig. 6a for the depth intervals 325-435 km and 435-560 km.

Table II. Representative parameters of the inversion of the two datasets.

Dataset	Eqs.	N. obs.	Data variance (s^2)	Remaining variance (s^2)	Variance improvement (%)	Damping (s^2)
$P + PKP_{df}$	107	4235	0.70	0.15	79	50
All Phases	107	7070	0.69	0.21	69	50

part of the alpine chain has been interpreted as lithospheric *roots* left from the continental collision which followed the Tethyan subduction, on the basis of surface wave analysis (Panza and Mueller, 1979). This interpretation also emerges from gravity studies (Kissling *et al.*, 1983) and travel-time studies (Babuška and Plomerová, 1990).

In layer 3 (85-150 km; fig. 6a, lower panels), the main feature of the reconstructed upper mantle velocity structure is represented by the presence of a high-velocity region that, especially in the *All Phases* image, appears continuously extending from the Central Alps through the Ligurian Apennines to the Central Apennines. As already proposed by Amato *et al.* (1993a,b), Cimini and Amato (1993), we interpret the positive velocity anomaly detected beneath the Northern Apennines as a remnant lithospheric slab formed by the westward Adriatic subduction beneath the Tuscany-Sardinia-Corsica block. The images obtained with the use of a more complete sampling of the mantle structure (the *All Phases* dataset) indicate that the high-velocity region is also present below Central Italy. The southern boundary of this positive anomaly, approximately coincides with the transition zone between the Northern and Central-Southern Apennines. Its absence beneath the Southern Apennines and the apparent non-continuity with the high-velocity zone that characterizes a wide area beneath Southern Italy from the Apulian foreland to Northern Sicily, confirm the differences in tectonic evolution undergone by the northern arc and Southern Apennines. This *slab window* may derive either from an irregular geometry of the two colliding plates or from a faster thermo-assimiliation of the southern part of the subducted Adriatic lithosphere below the Apennines (Amato *et al.*, 1993b).

Another important characteristic descending from the comparison of the velocity maps of layer 3, is the different imaging of the depth extent of the wide low-velocity region observed below the Po plain between 35-85 km of depth (fig. 6a, upper panels). The existence of low-velocity zones starting just below the Moho and extending down to depths ranging from 75 to 255 km, were hypothesized beneath the Po valley by Calcagnile *et al.* (1979) from dispersion analysis of Rayleigh waves. Our results show that at the lithospheric depths of layer 3, this feature is still imaged only in the $P+PKP_{df}$ panel, where it appears mostly concentrated beneath the easternmost part of the Po plain. By contrast, both the inversions recover quite similarly the low-velocity area beneath the perityrrhenian volcanoes of Tuscany, Latium, and Campania, suggesting in this case a more reliable feature of the upper mantle structure.

Finally, it is worth noting how the low-velocity zone observed beneath Central Sicily (see also layer 2), corresponds at the surface to a well-developed gravimetric minimum located in the Gela-Catania Foredeep region. The presence of this upper mantle low-velocity anomaly could suggest that the volcanism in this region has deep and extensive roots, although a more precise identification of the geometry and extension of the heterogeneous zone would require a denser array of seismic stations.

In layer 4 (150-230 km; fig. 6b, upper panels), the most prominent upper mantle anomalies are found beneath the Northern Apennines and Southern Tyrrhenian sea-Calabrian arc. The high-velocity zone in the lithosphere-asthenosphere system of the Northern Apennines is wider and more pronounced in

the *All Phases* panel, although the geographic distribution is similar to that observed in the $P+PKP_{df}$ image. Conversely, the Southern Tyrrhenian subduction zone appears differently recovered in the two velocity maps (high-velocity anomalies more concentrated below Northern Sicily in the case of $P+PKP_{df}$ inversion and below Calabrian arc for the *All Phases* inversion), suggesting a different resolving power of the two datasets. The next section will show how the inversion of both first and secondary *P* phases resulted in a significant improvement of the resolution, thus indicating the greater reliability of the *All Phases* tomographic images.

Layers 5 (230-325 km; fig. 6b, lower panels) to 7 (435-560 km; fig. 6c, lower panels) share the common feature that velocity anomalies recovered from the inversion of the first arrivals dataset, generally appear less pronounced in the *All Phases* model. Except for the region of high-velocity perturbations located beneath the Southern Tyrrhenian sea and Calabria (layer 6, fig. 6c), and the low-velocity anomaly beneath Sicily (layer 7, fig. 6c), the *All Phases* panels do not display at these depths the presence of strong heterogeneous zones in the well-resolved part of the target volume. In particular, the wide area of positive velocity changes observed in the bottom layer of our block model below the Central Tyrrhenian sea, results almost completely unrecovered in the *All Phases* tomogram. The existence of such a feature would be of extreme relevance for a better comprehension of the geodynamic evolution of the Tyrrhenian basin, because it would substantiate a bending below a depth of about 400 km of the Ionian lithosphere subducting from the Calabrian arc northwestward. As opposed to the $P+PKP_{df}$ results, the 3D inversion of both direct and secondary travel-time residual data does not seem to indicate a subhorizontal continuity at depth of the high-velocity body imaged beneath the Southern Tyrrhenian sea. This is better illustrated in fig. 7, where the pattern of the *P*-wave velocity anomalies is displayed on a NW-SE vertical section crossing the area under investigation from Corsica to the Ionian sea. Here, the slab reconstructed by inverting the

All Phases dataset appears subhorizontal until the Calabrian arc, then abruptly deepens down to 435 km offshore from the Calabrian arc. The image depicts a rather continuous high-velocity body that well correlates with the distribution of intermediate and deep earthquakes, although a decrease in the velocity contrast between the slab and the contiguous mantle (from ~ +7% to ~ +3.5%) is observed in correspondence of the depth interval of layer 5 (230-325 km). The coincidence of the seismicity with the region of positive velocity perturbations, already pointed out by previous tomographic studies (Spakman, 1990; Amato *et al.* 1993a,b; Selvaggi and Chiarabba, 1995), indicates that the subduction process of the oceanic Ionian plate beneath the Calabrian arc is still active.

4. Hit count, resolution and standard errors

The reliability of any tomographic image depends on two factors: the spatial resolution of the image and the standard error estimate of the model parameters. The hit count patterns (number of rays crossing the blocks in the model) quantify the sampling of the mantle by ray paths and provide a first qualitative measure of resolution. More effectively, model resolution can be visualized in terms of the resolution matrix, which specifies the mapping of the *true* Earth model into the estimated model parameters. Physically, the elements of the *j*-th column of the resolution matrix represents how the inverse operator spreads the *j*-th model parameter among the other model parameters (Menke, 1989). The largest non-zero values around the diagonal reveal the direction along which the anomaly for that block is smeared out into adjacent blocks.

Figure 8 shows the ray sampling of the investigated volume along the same cross-section of fig. 7, resulting from the $P+PKP_{df}$ and *All Phases* dataset, respectively. The illumination of the upper mantle beneath the Tyrrhenian sea and Calabrian arc obtained by adding ray-paths of later arriving P phases, appears greatly improved especially in the dipping direction of the slab. As shown in fig. 9 and table III, this leads to a significant reduction of vertical

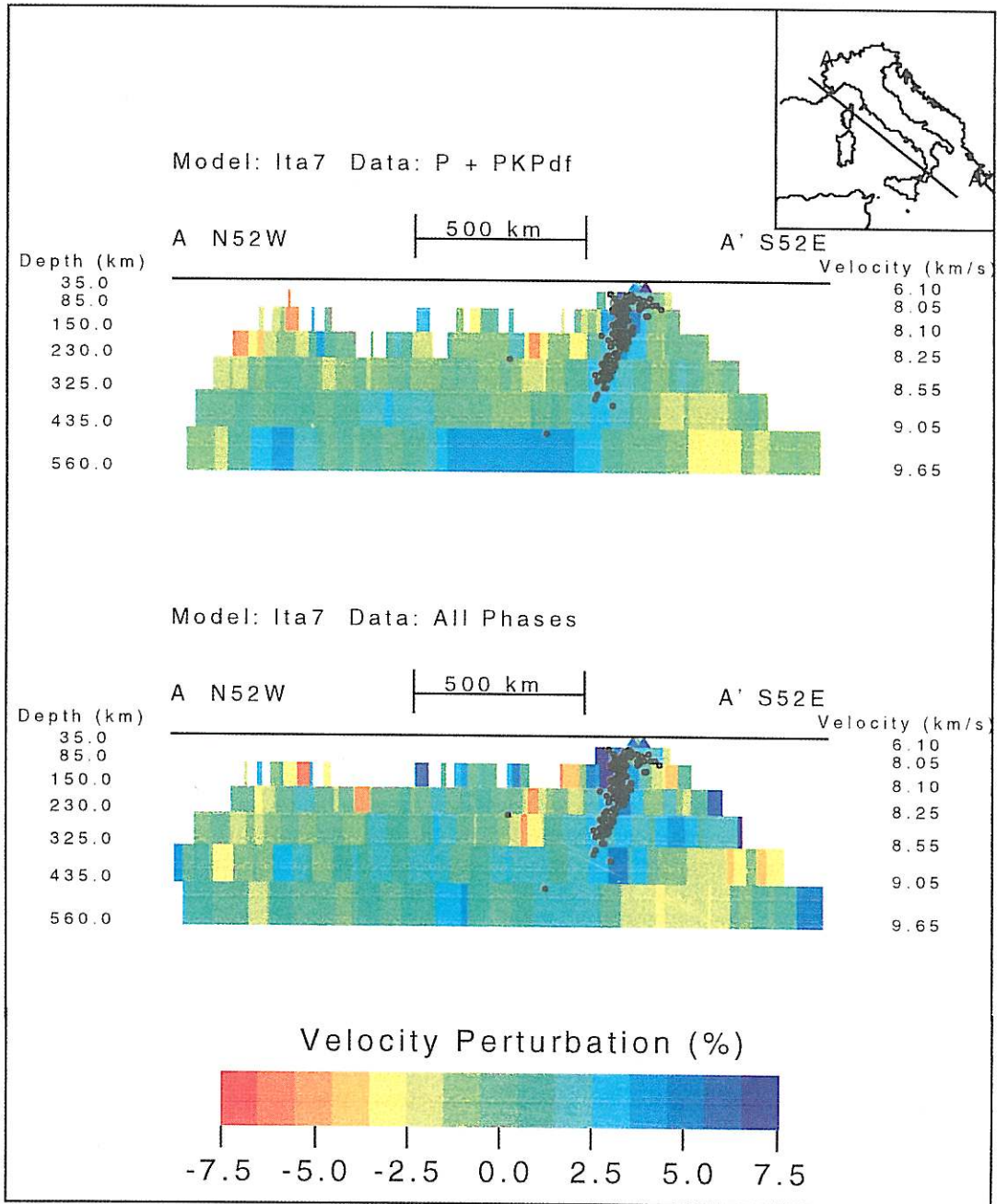**Fig. 7.** NW-SE vertical section through the model showing the different tomographic reconstruction of the deep high-velocity body beneath the Southern Tyrrhenian sea. Dots in the cross-sections denote subcrustal hypocenters from Selvaggi and Chiarabba (1995) located within ± 50 km of the vertical plane.
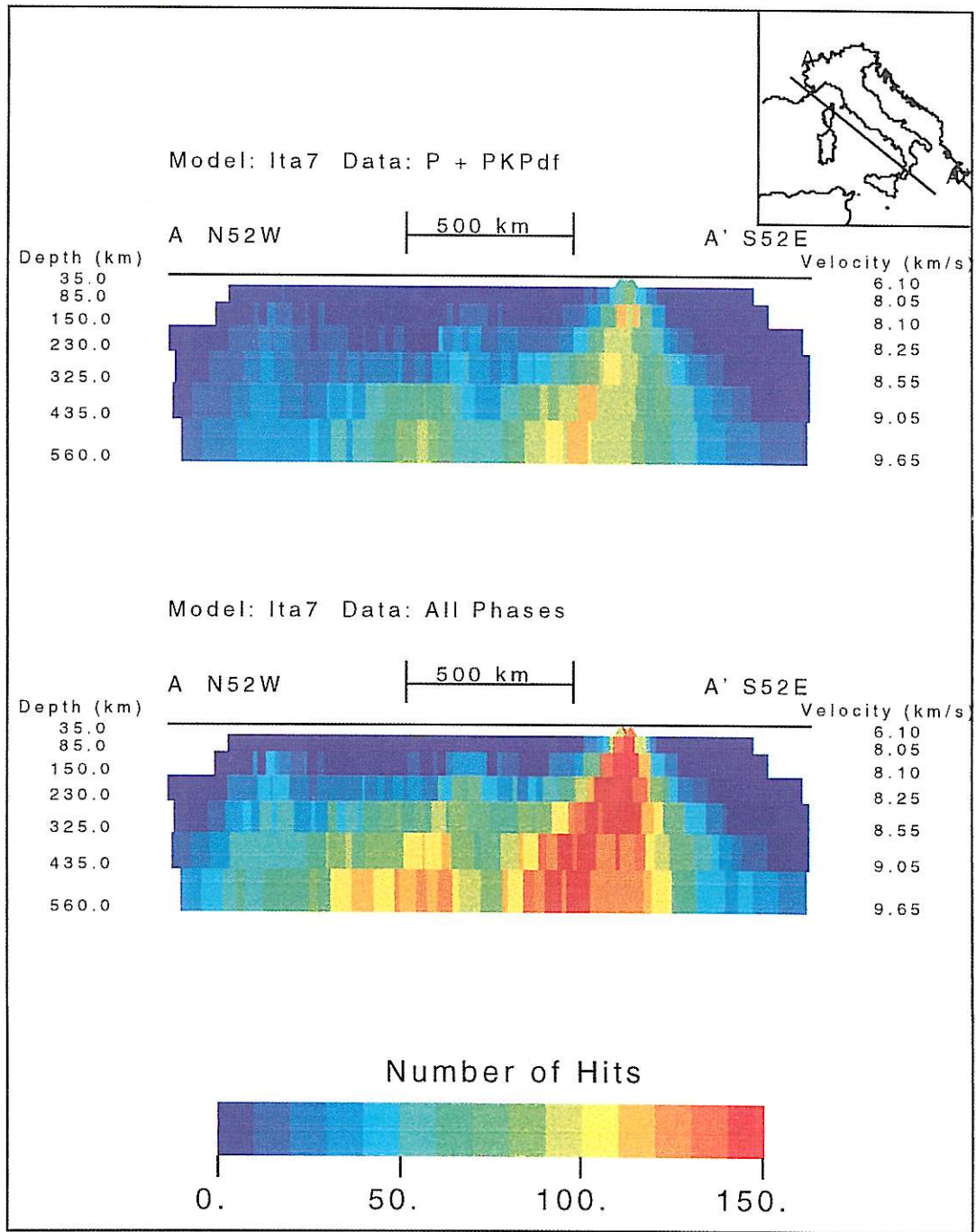
Fig. 8. Number of ray paths for the two datasets along the same vertical section as fig. 7.

Model: Ita7 Data: P + PKPdf

A N52W 500 km A' S52E

Depth (km)   Velocity (km/s)
35.0   6.10
85.0   8.05
150.0   8.10
230.0   8.25
325.0   8.55
435.0   9.05
560.0   9.65

Model: Ita7 Data: All Phases

A N52W 500 km A' S52E

Depth (km)   Velocity (km/s)
35.0   6.10
85.0   8.05
150.0   8.10
230.0   8.25
325.0   8.55
435.0   9.05
560.0   9.65

Resolution

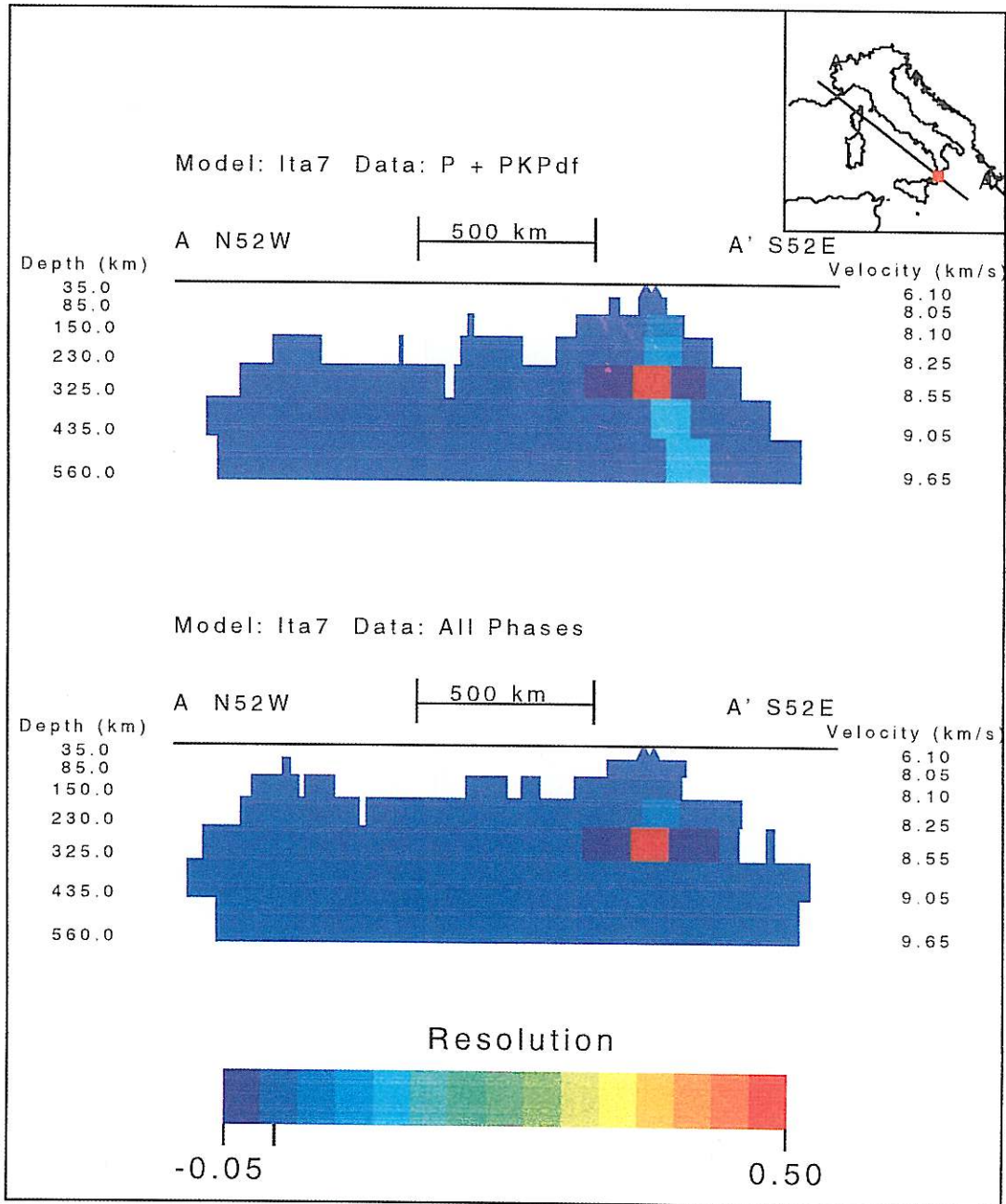-0.05   0.50

Fig. 9. Column of the resolution matrix (off-diagonal elements) for a *fast* block in the fifth layer, displayed along vertical section AA'. Inversion parameters for this block are listed in table III. The resolution values obtained by inverting the $P+PKP_{df}$ dataset witnessing a smearing of the velocity anomaly in the vertical direction.
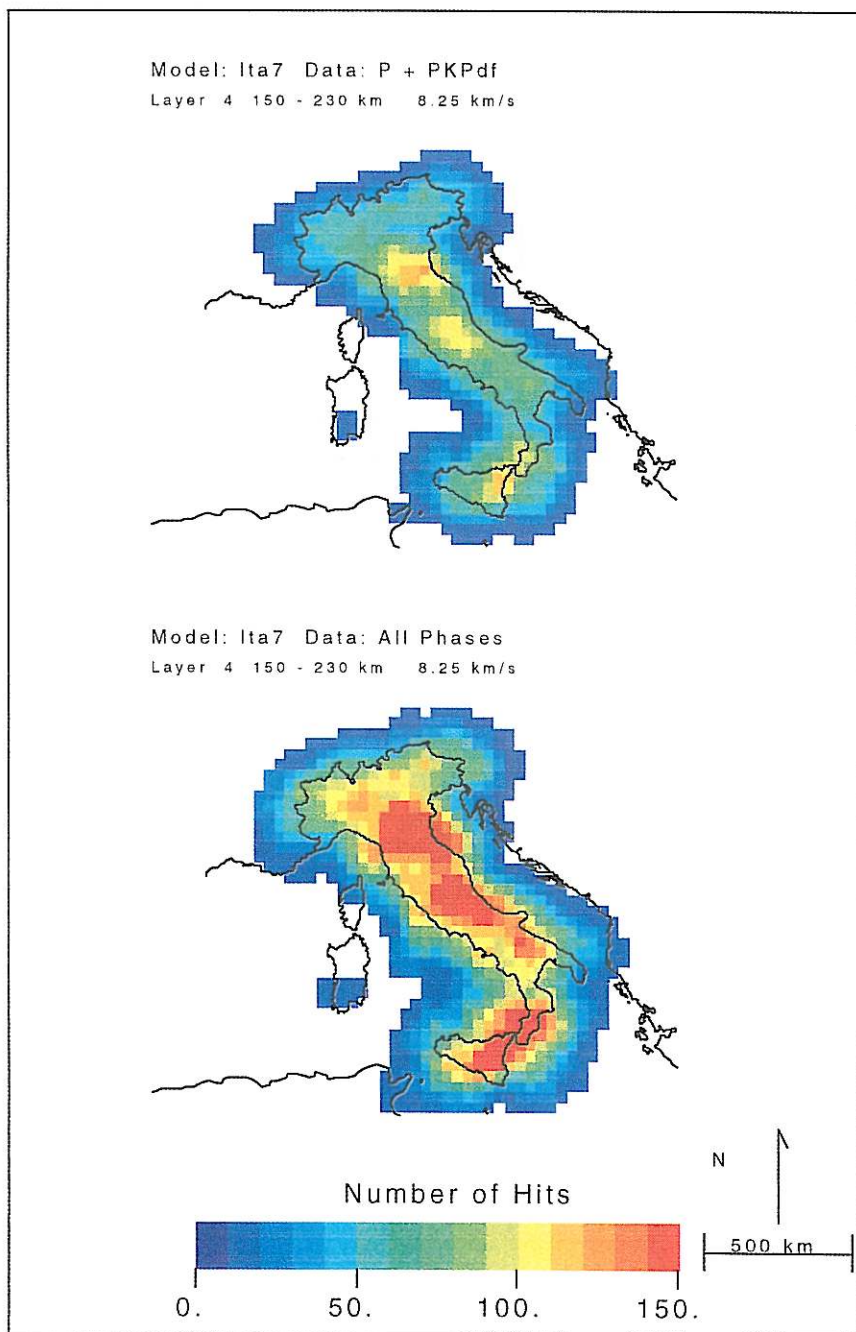
Fig. 10. Map view of the hit count, illustrating the sampling by $P+PKP_{df}$ (upper panel) and *All Phases* datasets (lower panel) of blocks in the fourth layer of the model.
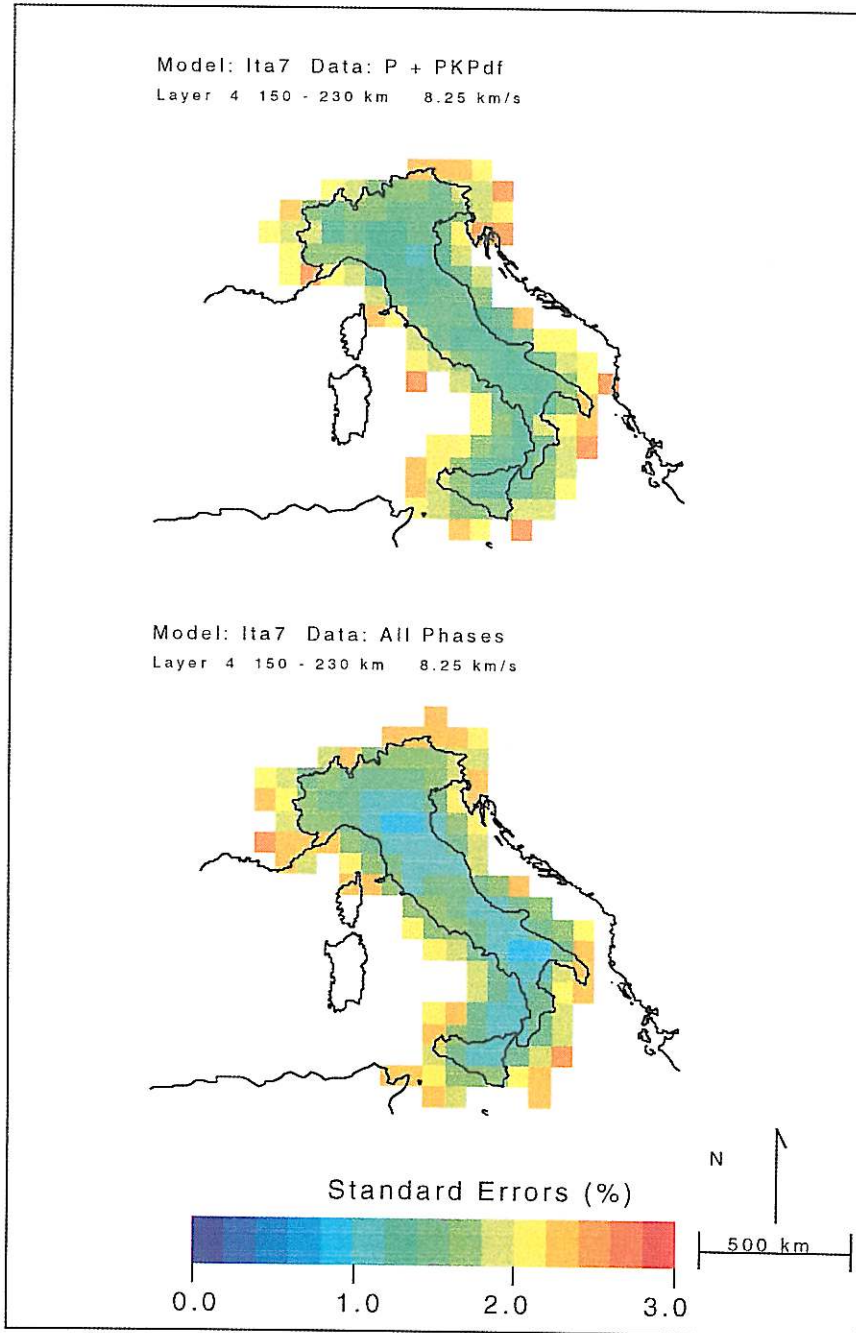
Fig. 11. Standard errors computed for velocity perturbations in the fourth layer. In the well-sampled part of model (see fig. 10) the values (smaller for the *All Phases* dataset) are, on average, of about 1.0-1.5%.

Table III. Inversion results for a high-velocity block of the model located in the upper mantle beneath the Calabrian arc between 230 and 325 km of depth (see also fig. 9).

Dataset	N. rays	Velocity perturbation (%)	Resolution (diagonal values)	Standard errors (%)
$P + PKP_{df}$	85	3.18	0.7844	1.32
All Phases	149	4.20	0.9505	1.22

smearing effects and, consequently, to a more reliable reconstruction of the geometry of the high-velocity body, characterised by no apparent bending at depths greater than ~ 450 km. Finally, we show in figs. 10 and 11 the hit count patterns and the standard errors associated to the velocity anomalies in the fourth layer of the cell model, respectively. As previously described, most of the lateral heterogeneities recovered by inversion of the *All Phases* dataset seem to be confined in the upper mantle between 35 km and the bottom of the fourth layer (230 km). A verification of the ray sampling and of the uncertainty on the model parameter estimates for blocks belonging to this layer, is then important for interpreting the differences between the two tomographic reconstructions. From fig. 10 we see that the *All Phases* dataset provides a more adequate illumination of the upper mantle structure, particularly beneath the Apenninic chain and Calabrian arc-Sicily, where both models delineate wide regions of high-velocity perturbations (see fig. 6b). The analysis of the standard errors, the square root of the diagonal elements of the *a posteriori* covariance matrix (Evans and Achauer, 1993), confirms the better significance of the velocity anomalies recovered from the *All Phases* inversion, showing standard errors that in the well-sampled blocks average about ± 1.25% (fig. 11). Most upper mantle anomalies interpreted in this study are greater than ± 4%, which is approximately three times this average uncertainty on the model parameters.

From this evidence and the fact that beyond the maximum depth of resolution, which in our case is about 250 km (this depth is roughly equal to the smallest dimension covered by the seismic network), the ray distribution significantly decreases (due to divergence of rays with depth), we conclude that inclusion of secondary *P* phases is essential in mitigating inversion artifacts caused by the limited vertical resolution of direct *P*-wave teleseismic tomography.

5. Conclusions

In this study we explored the effect of adding data of later arriving *P* phases in an ACH inversion (Aki *et al.*, 1977) for the aspherical velocity structure of the mantle below Italy. As the quality of data is a crucial point in damped least squares inversion procedure, we estimated the arrival times of both direct and secondary phases through a direct analysis of the original seismograms. Due to this analysis, the standard errors associated to the residual distributions of later phases are generally comparable with the travel-time residual variance of phases recorded as first arrivals (table I). Although the inversion results for the two datasets ($P+PKP_{df}$ and *All Phases*) are substantially consistent between them and with results of earlier investigations (Cimini and Amato, 1993), some important differences occur in the spatial extension, geometry and amplitude of the main heterogeneous zones. Particularly in the depth range 85-150 km, the *All Phases* images show a more continuous pattern of high velocity anomalies extending beneath the Western Alps and Northern-Central Apennines than the images based solely on the first arrivals dataset. Also, we obtained a different reconstruction of the Southern Tyrrhenian subduction zone, with no evidence in the *All Phases* images of a *spoon-shaped* geometry of the slab. These modifications are important if the tomographic images are used to constrain

geodynamic models of this portion of the Mediterranean.

Finally, the inclusion of seismic ray-paths that are oblique to rays of direct P phases significantly enhanced the spatial resolution of the upper mantle structure. Especially in areas not adequately sampled by P rays, we obtained a substantial reduction of the vertical smearing effects on the velocity anomalies, thus enhancing the better reliability of the new tomographic reconstructions.

Acknowledgements

REFERENCES

AKI, K., A. CHRISTOFFERSSON and E.S. HUSEBYE (1977): Determination of the three-dimensional seismic structure of the lithosphere, *J. Geophys. Res.*, **82**, 277-296.

AMATO, A., B. ALESSANDRINI and G.B. CIMINI (1993a): Teleseismic wave tomography of Italy, in *Seismic Tomography: Theory and Practice*, edited by H.M. IYER and K. HIRAHARA (Chapman and Hall, London), 361-397.

AMATO, A., B. ALESSANDRINI, G.B. CIMINI, A. FREPOLI and G. SELVAGGI (1993b): Active and remnant subducted slabs beneath Italy: evidence from seismic tomography and seismicity, *Annali di Geofisica*, **36** (2), 201-214.

BABUŠKA, V. and J. PLOMEROVÁ (1990): Tomographic studies of the upper mantle beneath the Italian region, *Terra Nova*, **2**, 569-576.

BULAND, R. and C.H. CHAPMAN (1983): The computation of seismic travel times, *Bull. Seism. Soc. Am.*, **73**, 1271-1302.

CALCAGNILE, G., G.F. PANZA and L. KNOPOFF (1979): Upper-mantle structure of North-Central Italy from the dispersion of Rayleigh waves, *Tectonophyiscs*, **56**, 51-63.

CHOY, G.L. and P.G. RICHARDS (1975): Pulse distortion and Hilbert transformation in multiply reflected and refracted body waves, *Bull. Seism. Soc. Am.*, **65**, 55-70.

CIMINI, G.B. and A. AMATO (1993): *P*-wave teleseismic tomography: contribution to the delineation of the upper mantle structure of Italy, in *Recent Evolution and*

Seismicity of the Mediterranean Region, edited by E. BOSCHI, E. MANTOVANI and A. MORELLI (Kluwer Academic Publishers, Dordrecht), 313-331.

CIMINI, G.B., C. CHIARABBA, A. AMATO and H.M. IYER (1994): Large teleseismic *P*-wave residuals observed at the Alban Hill volcano, Central Italy, *Annali di Geofisica*, **37**, 969-988.

DZIEWONSKY, A.M. and F. GILBERT (1976): The effect of small, aspherical perturbations on travel times and a re-examination of the corrections for ellipticity, *Geophys. J.R. Astron. Soc.*, **44**, 7-17.

EVANS, J.R. and U. ACHAUER (1993): Teleseismic velocity tomography using the ACH method: theory and application to continental-scale studies, in *Seismic Tomography: Theory and Practice*, edited by H.M. IYER and K. HIRAHARA (Chapman and Hall, London), 319-360.

GIARDINI, D. and M. VELONÀ (1991): The deep seismicity of the Tyrrhenian sea, *Terra Nova*, **3**, 57-64.

HILL, P.D. (1974): Phase shift and pulse distortion in body waves due to internal caustics, *Bull. Seism. Soc. Am.*, **64**, 1733-1742.

KENNETT, B.L.N. and E.R. ENGDAHL (1991): Travel times for global earthquake location and phase identification, *Geophys. J. Int.*, **105**, 429-465.

KISSLING, E., S. MUELLER and D. WERNER (1983): Gravity anomalies, seismic structure and geothermal history of the Central Alps, *Annales Geophysicae*, **1**, 37-46.

MENKE, W. (1989): *Geophysical Data Analysis: Discrete Inverse Theory*, Revised Edition (Academic Press, Inc., San Diego, California), pp. 289.

PANZA, G.F. and S. MUELLER (1979): The plate boundary between Eurasia and Africa in the Alpine area, *Mem. Sci. Geol.*, **33**, 43-50.

SELVAGGI, G. and A. AMATO (1992): Intermediate-depth earthquake in Northern Apennines (Italy): evidence for a still active subduction?, *Geophys. Res. Lett.*, **19**, 2127-2130.

SELVAGGI, G. and C. CHIARABBA (1995): Seismicity and *P*-wave velocity image of the Southern Tyrrhenian subduction zone, *Geophys. J. Int.*, **121**, 818-826.

SPAKMAN, W. (1990): Tomographic images of the upper mantle below Central Europe and the Mediterranean, *Terra Nova*, **2**, 542-552.

SPAKMAN, W., S. VAN DER LEE and R.D. VAN DER HILST (1993): Travel-time tomography of the European-Mediterranean mantle down to 1400 km, *Phys. Earth Planet. Int.*, **79**, 3-74.

SPAKMAN, W., S. STEIN, R.D. VAN DER HILST and R. WORTEL (1989): Resolution experiment for NW Pacific subduction zone tomography, *Geophys. Res. Lett.*, **16**, 1097-1100.

VAN DER HILST, R.D. and E.R. ENGDAHL (1991): On *ISC PP* and *pP* data and their use in delay-time tomography of the Caribbean region, *Geophys. J. Int.*, **106**, 169-188.

VAN DER HILST, R.D. and W. SPAKMAN (1989): Importance of the reference model in linearized tomography and images of subduction below the Caribbean plate, *Geophys. Res. Lett.*, **16**, 1093-1096.